LAWRENCE
LIVERMORE
NATIONAL
LABORATORY

LLNL-TR-405719

Comparison of Crevice Corrosion of Fe-Based Amorphous Metal and Crystalline Ni-Cr-Mo Alloy

X. Shan, H. Ha, J. H. Payer

July 25, 2008

Disclaimer

This work performed under the auspices of the U.S. Department of Energy by Lawrence Livermore National Laboratory under Contract DE-AC52-07NA27344.

Comparison of Crevice Corrosion of Fe-Based Amorphous Metal and Crystalline Ni-Cr-Mo Alloy

X. SHAN, H. HA, J.H. PAYER

Materials Science and Engineering Department,
Case Western Reserve University
Cleveland, OH 44106 USA

The crevice corrosion behaviors of an Fe-based bulk metallic glass alloy (SAM1651) and a Ni-Cr-Mo crystalline alloy (C-22) were studied in 4M NaCl at 100°C with cyclic potentiodynamic polarization and constant potential tests. The corrosion damage morphologies, corrosion products and the compositions of corroded surfaces of these two alloys were studied with optical 3D reconstruction, Scanning Electron Microscopy (SEM), Energy Dispersive Spectroscopy (EDS) and Auger Electron Spectroscopy (AES). It was found that the Fe-based bulk metallic glass (amorphous alloy) SAM1651 had a more positive breakdown potential and repassivation potential than crystalline alloy C-22 in cyclic potentiodynamic polarization tests and required a more positive oxidizing potential to initiate crevice corrosion in constant potential test. Once crevice corrosion initiated, the corrosion propagation of C-22 was more localized near the crevice border compared to SAM1651, and SAM1651 repassivated more readily than C-22. The EDS results indicated that the corrosion products of both alloys contained high amount of O and were enriched in Mo and Cr. The AES results indicated that a Cr-rich oxide

passive film was formed on the surfaces of both alloys, and both alloys were corroded congruently.

I. INTRODUCTION

In recent years, amorphous alloys that have large supercooled liquid region before crystallization and high resistance against crystallization have been developed, and this has enabled the production of bulk amorphous alloys in the thickness range of 1 to100 mm by using various casting processes.[1-4] These bulk amorphous alloys exhibit many useful properties, such as high mechanical strength and high corrosion resistance.[2, 5] In addition, Fe- and Co- based bulk amorphous alloys also show good soft magnetic properties which cannot be obtained from crystalline-type magnetic alloys.[2, 5] The high boron content of these Fe-Cr-Mo-C-B based amorphous alloys also makes them an effective neutron absorber and suitable for nuclear criticality control applications. These bulk amorphous alloys extend their possible applications and have attracted much attention as new materials in scientific and engineering fields. A recent review covers several classes of corrosion resistant amorphous alloys,[6] several Fe-based bulk amorphous alloys with high corrosion resistance have been reported.[7-11] Pang et al.[8, 9] reported that Fe-Cr-Mo-C-B based amorphous alloys had a corrosion rate of 10^{-3} to 10^{-2} mm/year in 1, 6 and 12 M HCl solutions at room temperature and did not suffer pitting corrosion even when the alloys were polarized anodically up to 1.0 V (Ag/AgCl) in 12 M HCl solution. Farmer reported that one of the Fe-Cr-Mo-C-B based amorphous alloy SAM1651 (Fe48Cr15Mo14B6C15Y2), also known as SAM7 showed much more resistance to corrosion in aggressive environments such as 5M $CaCl_2$ at 105°C than crystalline type 316L stainless steel and nickel-based alloy C-22.[12, 13] Farmer[14] also reported that the corrosion resistance of iron-based amorphous alloy SAM2x5 (Fe49.7Cr17.7Mn1.9Mo7.4W1.6B15.2C3.8Si2.4) was comparable to that of nickel-based crystalline

alloy C-22 in natural seawater at 30 and 90 °C. The bulk metallic glass exhibited thermal stability, and the corrosion resistance was maintained after prior exposure to temperatures up to the glass transition temperature (approximately 570°C).[14]

The Fe-based amorphous alloys can be applied as thermal-spray coating. The results of standard salt fog test of ASTM B 117 showed that the amorphous coatings were resistant to rusting in salt fog.[15] Unlike stainless steel and nickel-based corrosion resistant alloy which lose the high corrosion resistance when used as a thermal spray coating, the corrosion resistance of the amorphous thermal-spray coating is almost unchanged compared to the bulk alloy.[13, 14] Due to the low cost of the alloy compared to nickel-based alloys and the high corrosion resistance, the Fe-based bulk metallic glass alloy is of interest for commercial applications.

Alloy C-22 (UNS# N06022), a nickel-chromium-molybdenum (Ni-Cr-Mo) crystalline alloy, has high uniform corrosion resistance in oxidizing environments and superior corrosion resistance in reducing corrosion media. The crystalline alloy C-22 also exhibits excellent resistance to pitting and crevice corrosion in low pH, high chloride oxidizing environments. For both the Fe-based amorphous alloys and Ni-Cr-Mo crystalline C-22 alloy, the high corrosion resistance is due in large part to the formation of a Cr-rich oxide passive film on the surface.

For alloys that depend on the durability of a passive film for corrosion resistance, localized corrosion is an important degradation mode to be evaluated for corrosion performance over long exposure periods. The localized corrosion of C-22 has been examined by a number of researchers.[16-25] The objective of this work is to study and compare the localized corrosion behavior of an Fe-based bulk metallic glass SAM1651 and Ni-based crystalline alloy C-22.

II. MATERIALS AND METHODS

Two materials are compared in this study: Fe-based bulk metallic glass SAM1651 and Ni-Cr-Mo-based crystalline alloy C-22. The nominal compositions of these two alloys are shown in table I. The SAM1651 rods with a diameter of 4.2 mm were obtained from Oak Ridge National Lab (ORNL). They were made by drop-cast into a copper mold. The alloy C-22 was obtained from Haynes Inc.

For C-22, two specimen types were used. One was a Multiple Crevice Assembly (MCA) specimen[26] made from 2 mm thick plates and shown in Figure 1. A polytetrafluoroethylene (PTFE) tape covered multi-contacts Al_2O_3 ceramic crevice former was used in MCA crevice tests. The assembly was tightened with grade 2 titanium bolt and nut with an applied torque of 7.91 N-m (70 in-lbs). For comparison with the amorphous alloy, a C-22 cylindrical specimen with 6 mm diameter and 3 to 4 mm length was also used in the cyclic potentiodynamic polarization test and the constant potential crevice corrosion test. The length of the SAM1651 alloy specimen was 4 to 7 mm. For the SAM1651 and C-22 cylindrical specimens, a modified crevice assembly holder was made and is shown in Figure 2. The holder was made of grade 2 titanium, and a titanium bolt was used to apply the pressure on the crevice former and create crevice gap. The crevice former was made from 3.2 mm diameter high purity Al_2O_3 ceramic rod and had a length of 2.5 mm. The contact surface was ground with 600 grit SiC paper to obtain a flat surface. In the tests with the modified crevice assembly holder, the surface of the crevice former that contacted the specimen was covered with PTFE tape. Two crevice formers were used in the modified crevice assembly, and the applied torque was 1.0 N-m (9 in-lb). For both the MCA specimen and cylindrical specimen, the test surfaces were ground to 600 grit SiC paper and ultrasonically cleaned with methanol before the crevice tests.

The test solution was 4M NaCl prepared with American Chemical Society (ACS) certified grade chemical, and the test temperature was 100 °C. Standard three-electrode method was used to run the crevice corrosion test. The counter electrode was rare earth coated titanium wire and separated from

main compartment of the test cell with a fritted glass tube. The reference electrode was a saturated calomel electrode (SCE) that was kept at room temperature and linked to the test cell through a salt bridge. A Gamry PC4/750 potentiostat was used for cyclic potentiodynamic polarization test. In cyclic potentiodynamic polarization test, the solution was deaerated with argon, and the open circuit potential (OCP) of the specimen was monitored. When the change of the OCP was less than 1 mV/hour, the cyclic potentiodynamic polarization test was performed. The scan started from 50 mV below OCP and swept toward to more positive potential. The scan was reversed when the current density equaled or exceeded 5 mA/cm^2. The scan rate was 0.167 mV/sec. For both the cyclic potentiodynamic polarization tests and the constant potential crevice corrosion tests, the test cell was open to air through a water cooled condenser. For each test condition, the result was repeated 2 to 4 times for repeatability and reliability.

The corrosion morphology examination and Energy Dispersive X-Ray Spectroscopy (EDS) were performed on a FEI/Philips XL-30 Scanning Electron Microscope (SEM). Auger Electron Spectroscopy (AES) was performed on a Perkin-Elmer PHI680. The corrosion damage depth profiles and 3-D reconstruction were performed with an Alicona Imaging InfiniteFocus® Microscope.

III. RESULTS

A. *Cyclic Potentiodynamic Polarization*

Figure 3 shows the cyclic potentiodynamic polarization results of SAM1651 and C-22 in deaerated 4M NaCl at 100 °C assembled with PTFE-tape covered ceramic crevice formers. Both results were obtained on the creviced cylindrical specimens with assembly shown in Figure 2. The measured corrosion potential of SAM1651 was -0.640 to -0.580 V-SCE, and this was slightly higher than the corrosion potential of C-22 tested under the same condition, which had an average value of -0.650 V-SCE. The breakdown potential of SAM1651 was +0.280 to +0.340 V-SCE, while the breakdown

potential of C-22 was -0.110 to -0.060 V-SCE. The breakdown potential of SAM1651 was about 370 mV more positive than that of C-22. During the reverse scan, both alloys exhibited a hysteresis loop. The repassivsation potential of SAM1651 was +0.190 to +0.280 V-SCE, while the repassivation potential of C-22 was -0.130 to -0.190 V-SCE. The repassivation potential of SAM1651 was 390 mV more positive than that of C-22. Post examination showed that crevice corrosion formed under the crevice contacts for both alloys, and this confirmed the hysteresis loop formed during the reverse scan which is an indication of the formation of localized corrosion. The cyclic potentiodynamic polarization results indicate that SAM1651 has considerably higher localized corrosion resistance than C-22 at the more oxidizing potential range.

B. *Constant Potential Crevice Corrosion Test*

Based on the cyclic potentiodynamic polarization results of alloy C-22 in 4M NaCl, 100 °C solution, -0.150 V-SCE was first used as the potential for the constant potential crevice corrosion tests. Figure 4 shows the current vs. time relationship in the -0.150 V-SCE constant potential crevice test of SAM1651 and C-22 in 4M NaCl 100 °C solution with PTFE tape covered ceramic crevice formers. Both alloys were tested with cylindrical specimens and the same size crevice formers. During the 28-day tests, the corrosion current of SAM1651 remained at less than 0.1 μA, and no indication of initiation of crevice corrosion was observed. Post-test examination of the SAM1651 specimen also confirmed that no corrosion initiated on either the alloy surface exposed to solution directly or on the alloy surface under the crevice formers. The SAM1651 specimen surface remained shiny metallic as before the test. While for C-22, crevice corrosion initiated and four crevice corrosion development stages can be identified from the current vs. time curve: incubation, propagation, stifling and arrest. After the anodic potential of -0.150 V-SCE was applied, crevice corrosion of the C-22 specimen

initiated in less than 5 minutes as indicated by the sharp increase of the corrosion current, and the minimum current before the initiation of crevice corrosion was 0.75 to 1.1 μA. After the initiation of the crevice corrosion, the overall corrosion current increased with increasing the test time, and maximum corrosion current of 30 μA was reached after 500 hours of exposure. During the propagation period, the corrosion current of C-22 showed multiple initiation/arrest events as indicated by current rise/drop serrations along the curve. After 580 hours of test, the corrosion current of C-22 dropped to 0.07 μA and showed an overall tendency to decrease with increasing test time. This indicates that the C-22 specimen became repassivated. The repassivation behavior of C-22 after extended corrosion has also been reported in other studies.[24, 27]

With increasing the test potential to +0.150 V-SCE, crevice corrosion initiated on SAM1651 specimen. Like C-22, four stages of damage evolution are indicated in the corrosion process of SAM1651: incubation, propagation, stifling and arrest. Figure 5 shows the current vs. time curve for SAM1651 tested under +0.150 V-SCE in 4M NaCl 100 °C solution. During the test, the maximum corrosion current was approximately 15 μA, which was still lower than that for the C-22 specimen tested under -0.150 V-SCE. During the 28 days of test, the total amount of charge to the SAM1651 specimen was 1.77 coulombs, compared to 30 coulombs for C-22 specimen tested under -0.150 V-SCE. The SAM1651 tested under more severe oxidizing condition exhibited a corrosion rate significantly lower than that of C-22. After testing for 600 hours, the corrosion current of SAM1651 dropped to below 0.1 μA. This indicates that SAM1651 became repassivated. The constant potential test results indicate that SAM1651 has higher localized corrosion resistance than C-22 at more oxidizing conditions. For SAM1651, a higher oxidizing potential was required to initiate crevice corrosion, and when localized corrosion initiated, it repassivated more readily for SAM 1651 than for C-22.

C. *Corrosion Morphology*

Figure 6a and 6b show the optical corrosion morphologies of SAM1651 and C-22 after similar amounts of corrosion. In Figure 6a, the corrosion products of SAM1651 specimen were still on the surface, while most of the corrosion products on the C-22 specimen in Figure 6b had been removed before the photograph was taken. For SAM1651 in Figure 6a, the specimen was tested at +0.150V-SCE in 4M NaCl 100°C solution for 211 hours, and the total amount of charge flowed to the specimen was 0.77 coulomb. Since there were two crevice formers with the specimen and no corrosion on the surface exposed to the test solution directly, the average amount of charge to each corroded crevice contact was 0.39 coulombs. For the C-22 specimen in Figure 6b, the test was performed on MCA specimen at -0.150 V-SCE in 4M NaCl 100°C solution for 90.5 hours, and the amount of charge to the specimen during the test was 1.0 coulomb. Since only one contact from the 12 crevice contacts of the crevice former was corroded during the test period, the amount of charge to the corroded contact of the MCA C-22 specimen was equal to the charge to the whole specimen. The crevice corrosion of SAM1651 initiated at locations under the crevice former and about 0.2 mm from the edge of the crevice contact. For C-22, the crevice corrosion also initiated under the crevice former, but nearer the edge of the crevice contact.

For each alloy, the crevice corrosion propagated both along the crevice and into the alloy. However, the corrosion penetration rate of C-22 into the alloy was higher than that of SAM1651, and the corrosion damage distribution of C-22 was more localized. At the end of the crevice corrosion test, the center region of the C-22 crevice contact was not corroded as shown in Figure 6b. The corroded area on the C-22 specimen after 1.0 coulomb of corrosion had a width of about 0.64 mm, a surface area of 4.8 mm^2, and the maximum corrosion penetration into the alloy was 25 μm located at about 0.1 mm

from the edge of the crevice contact. For the SAM1651 specimen after 0.77 coulomb of corrosion, except the outer 0.2 mm region, all the other surfaces under the crevice contacts were corroded including the center region. The corroded area of SAM1651 had a radius of 1.3 to 1.4 mm and surface area of 10 to 11 mm^2 (sum of two crevice contacts), and the corrosion penetration depth into the alloy was less than 5 μm. For similar amount of corrosion, the crevice corrosion of SAM1651 propagated further along the crevice and caused larger corroded area, while the maximum corrosion penetration into the SAM1651 alloy was more than 5 times less than that of C-22. Compared to SAM1651, the crevice corrosion propagation of C-22 was more localized near the crevice edge.

The more localized crevice corrosion of C-22 can also be observed on the cylindrical C-22 specimen tested with the same crevice former as SAM1651. Figure 6c shows the corrosion morphology of a cylindrical C-22 specimen, the current vs. time curve of this specimen is shown in Figure 4b, and the total amount of corrosion was 30 coulombs. There were two crevice contacts, and the amount of corrosion of each crevice contact was 15 coulombs on average. As can be seen from Figure 6c, in the center region of the C-22 crevice contact, there was still un-corroded region even though this cylindrical C-22 has higher amount of corrosion compared to the SAM1651 specimen shown in Figure 6a. The corroded area was 9.4 mm^2 (sum of two crevice former contacts), which was slightly less than that of SAM1651 with 0.77 coulomb of corrosion shown in Figure 6a. The maximum corrosion penetration into the C-22 specimen was 485 μm. Compared to SAM1651, the maximum corrosion penetration depth of C-22 increased hundreds of times while the amount of corrosion increased 39 times.

Figure 7 shows higher magnification of the surface morphology of the corroded area of SAM1651 and C-22 shown in Figure 6a and 6b. For SAM1651, the corrosion morphology consisted of many larger pits with a diameter of several μm and smaller pits with a diameter of sub-micron as shown in

Figure 8a and 8b. Spherical particles were observed on the surface of SAM1651 as shown in Figure 8b. AES analysis showed that these particles contained high concentrations of Y and O in the ratio of Y_2O_3. It is likely that these oxide particles were present in the melt prior solidification of the alloy. During the corrosion process, the substrate around the particles was corroded and the larger pit morphology formed. The surfaces within the larger pits were composed with the sub-micron pits as on the normal surfaces. The sub-micron pits are the typical corrosion morphology of the amorphous alloy.

For C-22, a characteristic of the corroded surface is that the grain boundaries were discernible as shown in figure 7b, and this was categorized as type I corrosion morphology of C-22 by Rebak.[28] The depth of the grain boundary penetration of C-22 was slight. Another characteristic of the corroded surface of C-22 is that the corroded surface was composed with many shallow pits with the diameter of several μm or less, and the surface of the pits was smooth. This type of C-22 corrosion morphology was categorized as type II corrosion morphology by Rebak.[28] Both types of corrosion morphologies of C-22 are related to its crystalline structure.[28]

D. *Corrosion Products*

After crevice tests where crevice corrosion occurred, black corrosion products were found under the crevice contacts for both SAM1651 and C-22 specimens. Figure 9 and Figure 10 show the morphologies and compositions of the corrosion products of SAM1651 and C-22 respectively. The smooth surfaces of the corrosion products shown were in contact with the PTFE tape covered crevice former. The corrosion products of these two alloys were similar both in morphology and composition, and both showed similar crack patterns through the corrosion products. For both alloys, the corrosion products contained high amount of O, and were enriched in Mo and Cr. The corrosion products of C-22 were also enriched in W. For SAM1651, the corrosion products were depleted in Fe, while for C-22, the corrosion products were depleted in Ni. Based upon E-pH (Pourbaix) diagrams, W, Mo and Cr

can form stable oxides in highly acidic environments, while Fe and Ni form soluble corrosion products in highly acidic environments. The former elements are primarily retained within the corroded crevice, while the latter elements diffuse/migrate out of the crevice and into the bulk test solution. More detailed analysis of the corrosion products of C-22 has been presented.[25]

E. *Element distribution of the corroded surface*

Figure 11 shows the composition depth profile on the corroded surface of SAM1651 and C-22 under the crevice contacts. The analyses were in areas of crevice corrosion, and the loosely adhered, bulk corrosion products had been removed from the surface to expose the repassivation at metal. For both alloys, high amounts of oxygen were found in the outer layers with nickel depletion from C-22 and iron depletion from SAM1651 surfaces, respectively. The analysis indicates a Cr-rich oxide layer (passive film) was formed on the surfaces. From the oxygen concentration changes, the passive film thickness on corroded SAM1651 surface is estimated to be about 15 to 20 nm, while the passive film thickness on corroded C-22 surface is estimated to be approximately 10 nm. The high corrosion resistance of these two alloys is due the passive film formed on the surface. It can also be seen from the figures that the composition of the bulk composition is observed beneath the oxide layer for both alloys. This indicates that both alloys were corroded congruently under the crevice, i.e. all of the elements in the alloy went into react at the same atomic percentages as the bulk alloy. Some elements were incorporated in solid products that remained within the crevice, while others were transported out of the crevice.

IV. CONCLUSIONS

The crevice corrosion behavior of Fe-based bulk metallic glass SAM1651 and crystalline Ni-Cr-Mo alloy C-22 are compared in high temperature (100°C), concentrated brine (4M NaCl) by cyclic potentiodynamic polarization and constant potential crevice corrosion tests.

1. SAM1651 has a more positive breakdown potential and repassivation potential than C-22.
2. SAM1651 needs more positive oxidizing potential to initiate crevice corrosion than C-22.
3. Once the crevice corrosion is initiated, SAM1651 repassivated more readily than C-22.
4. The crevice corrosion propagation of C-22 is more localized compared to SAM1651 bulk metallic glass amorphous.
5. The corrosion products of two alloys have similar morphology and composition. Both have high amount of O and are enriched in Mo and Cr. For SAM1651, the corrosion products are depleted in Fe, while for C-22 the corrosion products are depleted in Ni.
6. A chromium-rich oxide, passive film is observed on the surfaces of both alloys in corroded regions that had repassivated.
7. In regions where crevice corrosion was observed, both alloys are corroded congruently.

ACKNOWLEDGEMENTS

The work is carried out under the U.S. Department of Energy (DOE), Corrosion and Materials Performance Cooperative, DOE Cooperative Agreement Number: DE-FC28-04RW12252. The work is in support of the Defense Advanced Research Projects Agency, Defense Science Office, and the DOE Science & Technology Program of the Office of the Chief Scientist, Office of Civilian Radioactive Waste Management program for development of corrosion resistance of iron-based amorphous metal coatings under direction of Dr. J. C. Farmer at Lawrence Livermore National Laboratory.

REFERENCES

1. A. Inoue: Acta Mater., 2000, vol.48, pp. 279-306.

2. A. Inoue, B. Shen and A. Takeuchi: Mater. Sci. Forum, 2007, vol. 539-543, pp. 92-99.

3. V. Ponnambalam, S. J. Poon, and G. J. Shiflet: J. Mater. Res., 2004, vol. 19, pp. 1320-23.

4. V. Ponnambalam, S. J. Poon, and G. J. Shiflet: J. Mater. Res., 2004, vol. 19, pp. 3046-52.

5. A. Inoue, B. Shen, and A. Takeuchi: Mater. Sci. Eng. A, 2006, vol. 441, pp. 18-25.

6. J. R. Scully and A. Lucente: *ASM Handbook*, vol. 13B, ASM International, Materials Park, OH, 2005, pp. 476-489.

7. K. Asami, S.-J. Pang, T. Zhang, and A. Inoue: J. Electrochem. Soc., *2002,* vol. 149, pp. B366-B369.

8. S. J. Pang, T. Zhang, K. Asami, and A. Inoue: Corros. Sci., 2002, vol. 44, pp. 1847-56.

9. S. J. Pang, T. Zhang, K. Asami, and A. Inoue: Acta Mater., 2002, vol. 50, pp. 489–497.

10. J. Jayaraj, K. B. Kim, H. S. Ahn, and E. Fleury: Mater. Sci. Eng. A: 2007, vol. 449-451, pp. 517-520

11. J. Scully, A. Gebert, and J. H. Payer: J. Mater. Res., 2007, vol. 22, pp. 302-313.

12. J. Farmer, J. Haslam and et al: ECS Trans., 2007, vol. 3 (31), pp. 485-496.

13. J. C. Farmer, D. J. Branagan, C. A. Blue, J. D. K. Rivard, L. F. Aprigliano, N. Yang, J. H. Perepezko, and M. B. Beardsley. Corrosion Characterization of Iron-Based High-Performance Amorphous-Metal Thermal-Spray Coatings, (Paper presented at the 2005 ASME Pressure Vessels and Piping Division Conference, Denver, Colorado, 17-21 July 2005).

14. J. C. Farmer, J. J. Haslam, S. D. Day, T. Lian, C. K. Saw, P. D. Hailey, J.-S. Choi, R. B. Rebak, N. Yang, J. H. Payer, J. H. Perepezko, K. Hildal, E. J. Lavernia, L. Ajdelsztajn, D. J. Branagan, E. J. Buffa, and L. F. Aprigliano: J. Mater. Res., 2007, vol. 22, pp. 2297-2311.

15. R. B. Rebak, L. F. Aprigliano, S. D. Day, and J. C. Farmer: Materials Research Society Symposium Proceedings 985, 2007, pp.321-326.

16. G. O. Ilevbare: Corrosion (Houston, TX, U. S.), 2006, vol. 62, pp 340-356.

17. K. J. Evans, A. Yilmaz, S. D. Day, L. Wong, J. C. Estill, and R. Rebak: JOM, 2005, vol. 57, pp. 56-61.

18. B. A. Kehler, G. O. Ilevbare, and J. R. Scully: corrosion (Houston, TX, U. S.), 2001, vol. 57, pp. 1042-1065.

19. P. Pharkya, X. Shan, and J. H. Payer: ECS Trans., 2007, vol. 3(31), pp. 473-484.

20. D. Zagidulin, P. Jakupi, B. Sherar, J. J. Noel, and D. W. Shoesmith: ECS Trans., 2007, vol. 3(31), pp 419-430.

21. P. Jakupi, D. Zagidulin, J. Noël, and D. W. Shoesmith: ECS Trans., 2007, vol. 3(31), pp. 259-271.

22. M. Miyagusuku and T. M. Devine, CORROSION/2007, NACE International, Houston, TX, 2007, paper no. 07586.

23. A. S. Agarwal, U. Landau, X. Shan, and J. H. Payer: ECS Trans., 2007, vol. 3(31), pp. 459-471.

24. X. Shan and J. H. Payer: CORROSION/2007, NACE International, Houston TX, 2007, paper no. 07582.

25. X. Shan and J. H. Payer: ECS Trans., 2007, vol. 3(31), pp. 333-341.

26. Annual Book of ASTM Standards, 2005, vol. 03.02, ASTM International, West Conshohocken, PA, G48-03.

27. K. G. Mon, G. M. Gordon, and R. Rebak: Stifling of Crevice Corrosion in Alloy 22, (Paper presented at the 12th International Conference on Environmental Degradation of Materials in Nuclear Power System-Water Reactors, Salt Lake City, Utah, 14-18 August 2005).

28. R. Rebak: CORROSION/2005, NACE International, Houston, TX, 2005, paper no. 05610.

Table I. Nominal Composition of SAM1651 and Alloy C-22

Alloys	B	C	Cr	Mo	W	Y	Co	Fe	Ni
SAM1651, at%	6	15	15	14	0	2	0	48	0
SAM1651, wt%	1.2	3.4	14.9	25.7	0	3.4	0	51.3	0
C-22, at%	0	0	24.7	8.4	0.9	0	2.2	4.2	59.6
C-22, wt%	0	0	21	13.1	2.8	0	2.1	3.8	57.2

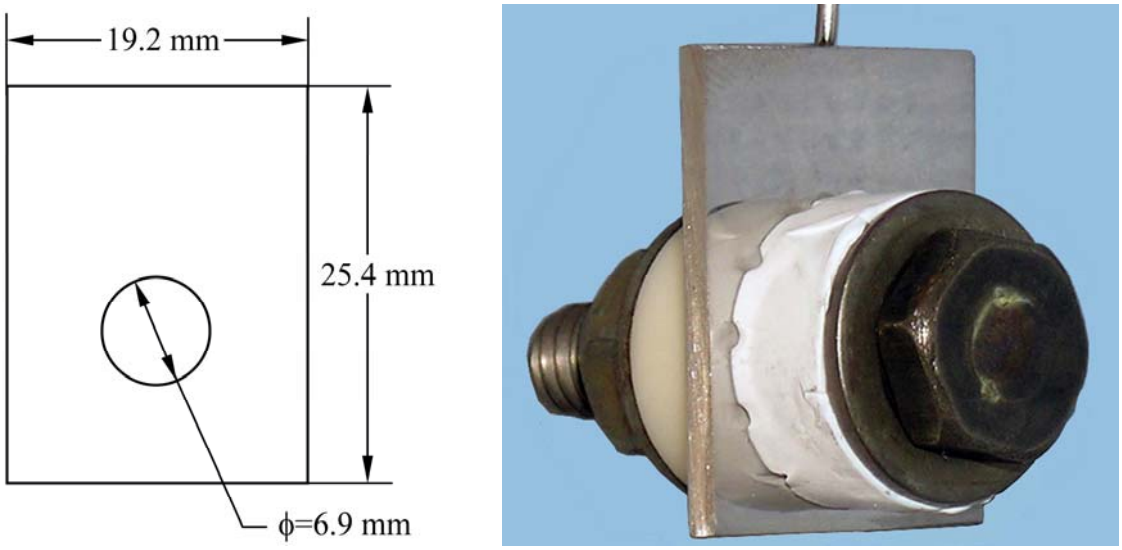

(a) (b)

Fig. 1: Multiple Crevice Assembly (MCA) (a) dimensions of MCA specimen (b) specimen assembly

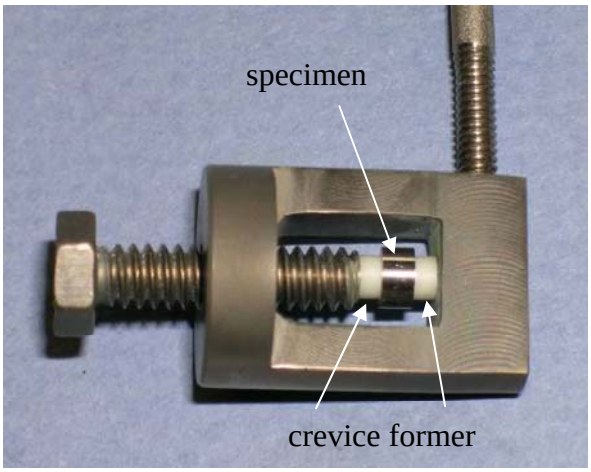

Fig. 2: Modified crevice corrosion test assembly for cylindrical specimen

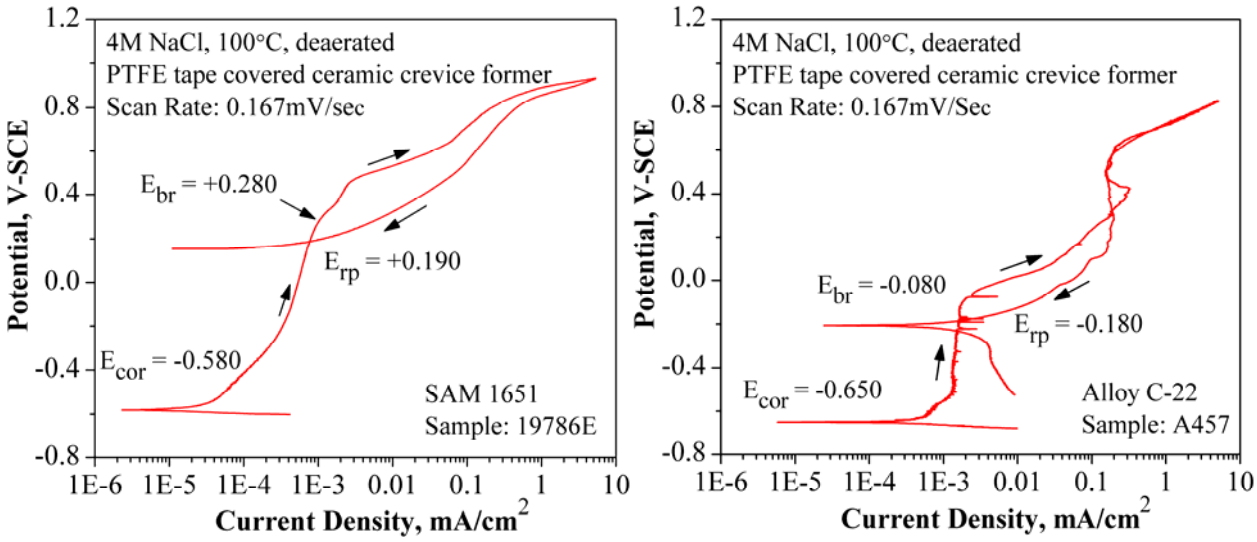

(a) (b)

Fig. 3: Cyclic potentiodynamic polarization curve of (a) SAM1651 cylindrical specimen and (b) C-22 cylindrical specimen in 4M NaCl 100 °C solution, deaerated

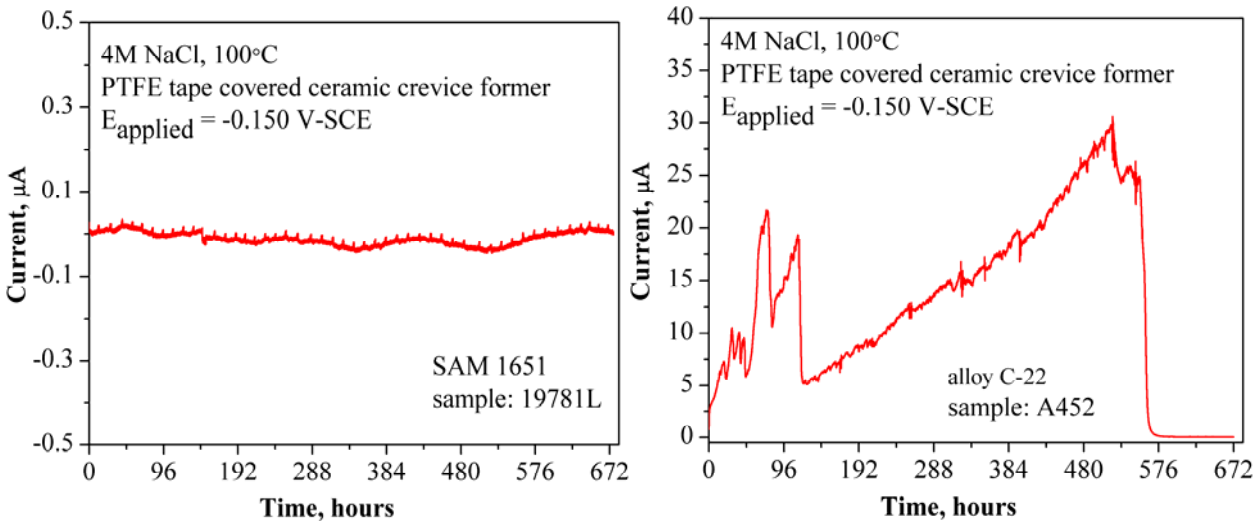

(a) (b)

Fig. 4: Constant potential crevice tests with (a) SAM1651 and (b) C-22 in 4M NaCl 100 °C solution, E=-0.150 V-SCE. Note the current for SAM1651 remained in the passive range throughout the test, i.e. I < 0.1 µA.

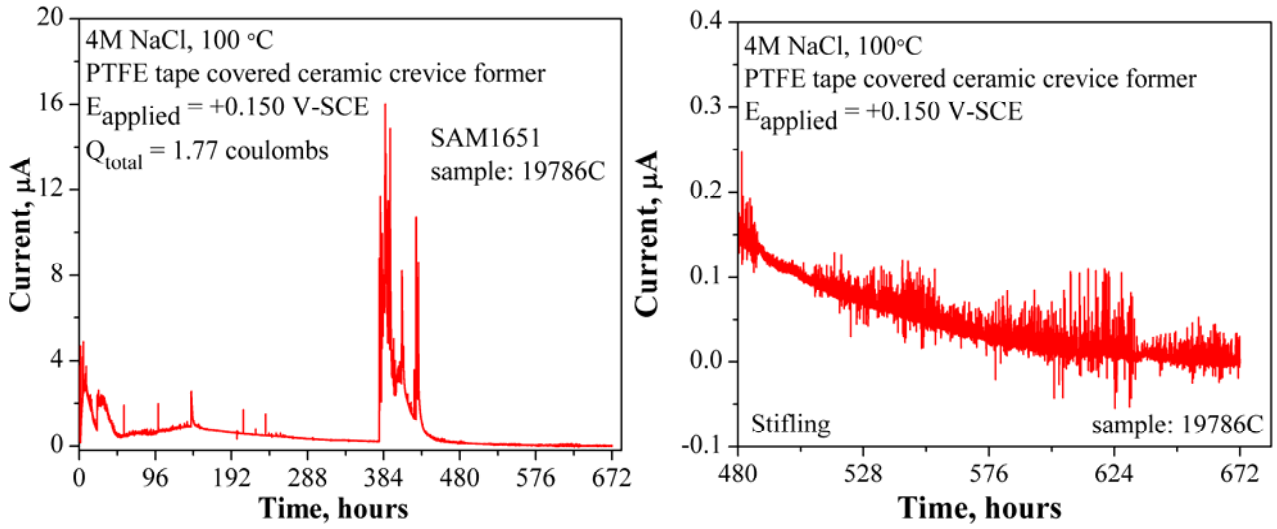

(a) (b)

Fig. 5: Constant potential crevice test with SAM1651 in 4M NaCl 100 °C solution, E=+0.150 V-SCE (a) entire time (0 to 672 hours) (b) later stage after repassivation (480 to 672 hours)

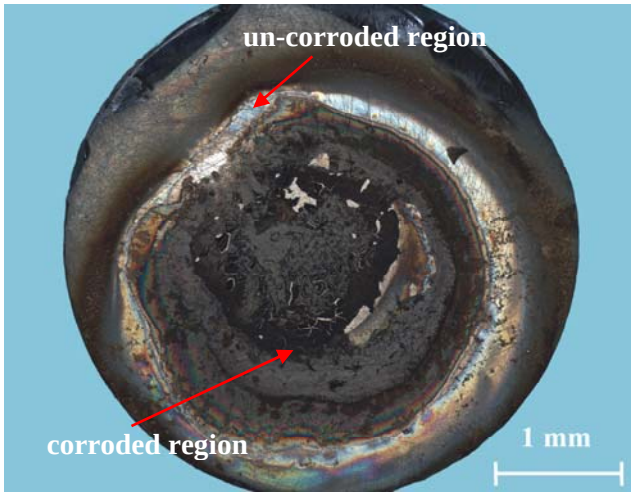

(a)

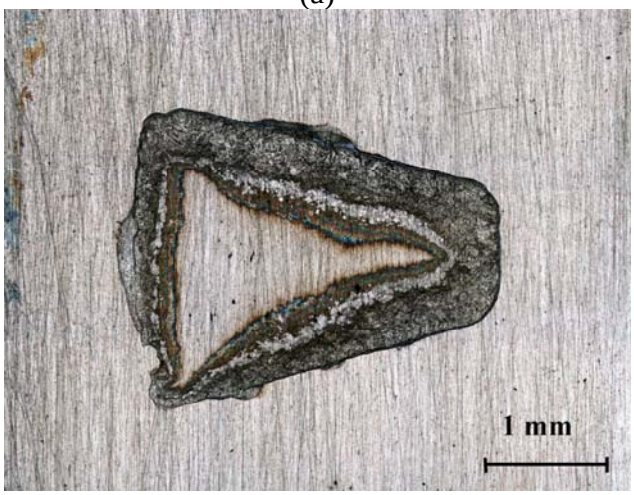

(b)

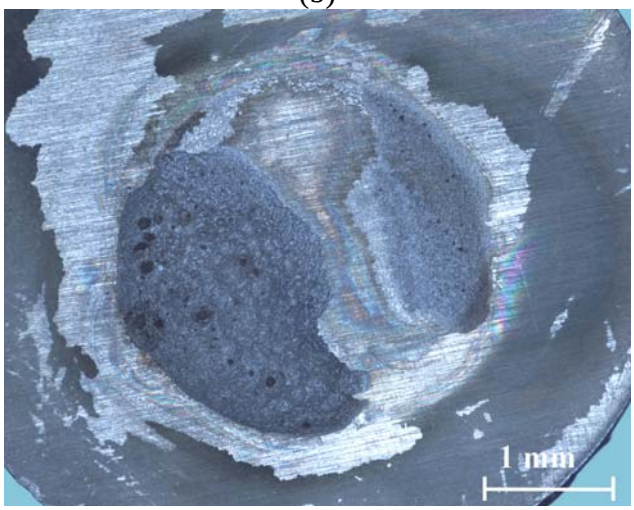

(c)

Fig. 6: Corrosion morphology of (a) SAM1651, E= +0.150 V-SCE, Q_{total} = 0.77 coulomb and (b) MCA C-22, E=-0.150 V-SCE, Q_{total} = 1.0 coulomb (c) cylindrical C-22, E=-0.150 V-SCE, Q_{total} = 30 coulombs after crevice corrosion tests in 4M NaCl, 100 °C

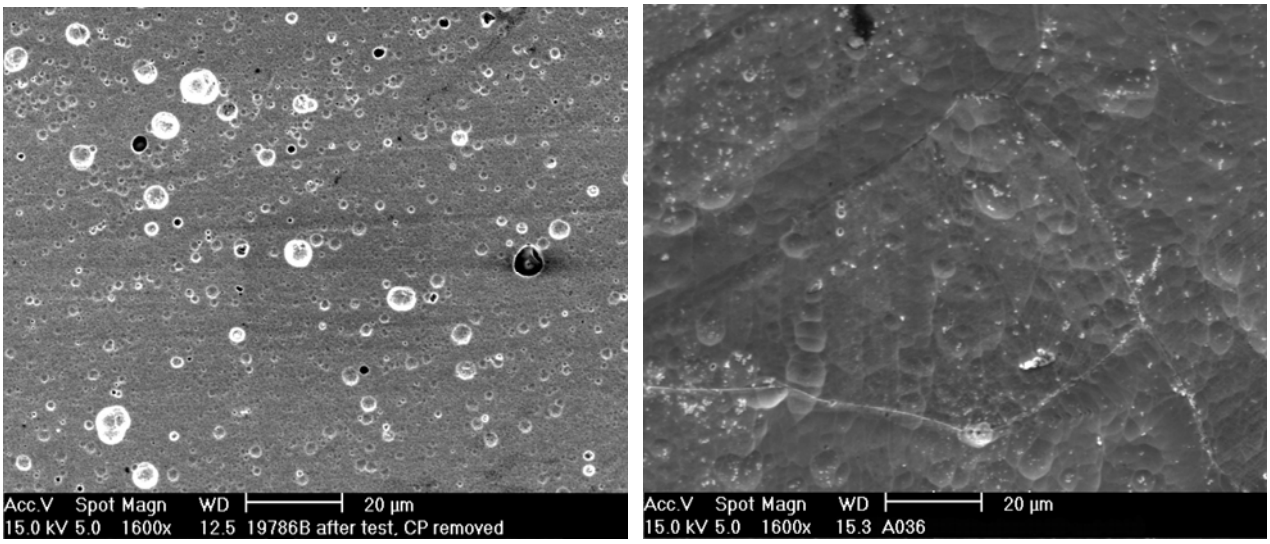

(a) (b)

Fig. 7: Corrosion morphologies of (a) SAM1651, E= +0.150 V-SCE, Q_{total} = 0.77 coulomb and (b) C-22, E=-0.150 V-SCE, Q_{total} = 1.0 coulomb after crevice corrosion tests in 4M NaCl, 100 °C

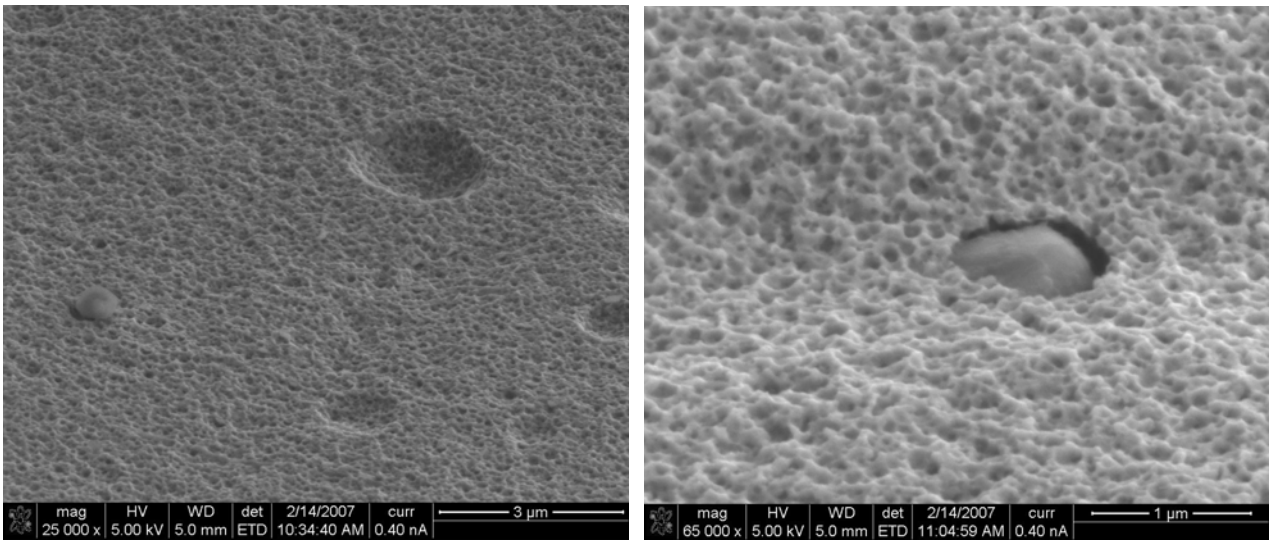

(a) (b)

Fig. 8: Higher magnification corrosion morphology of SAM1651 after crevice test (a) corroded surface (b) corroded surface and inclusion

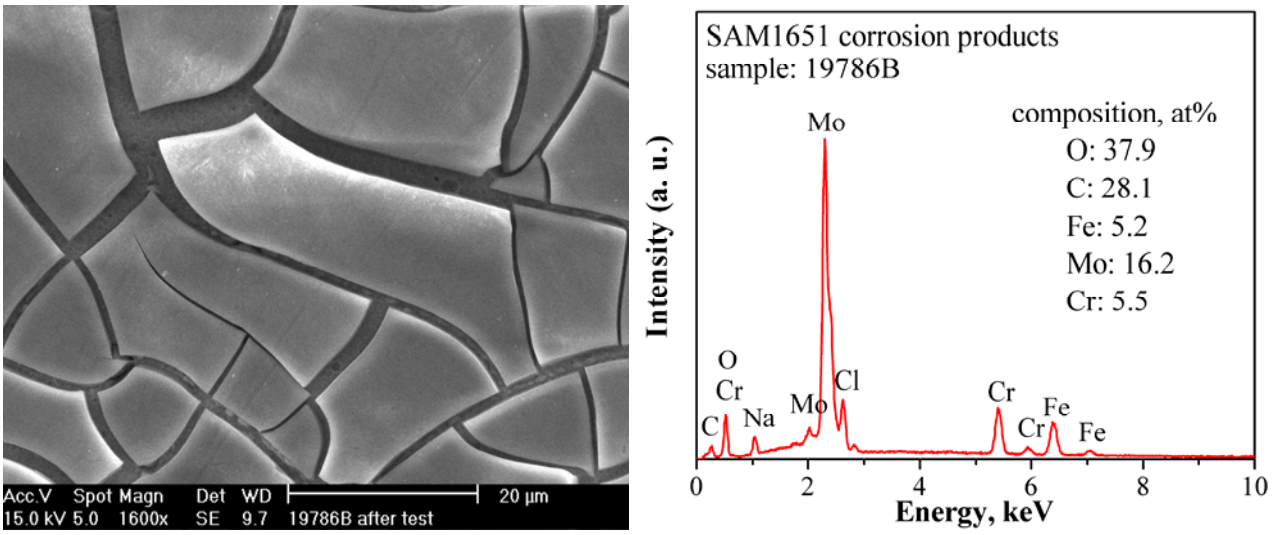

Fig. 9: SEM and EDS analysis of SAM1651 corrosion products under crevice former

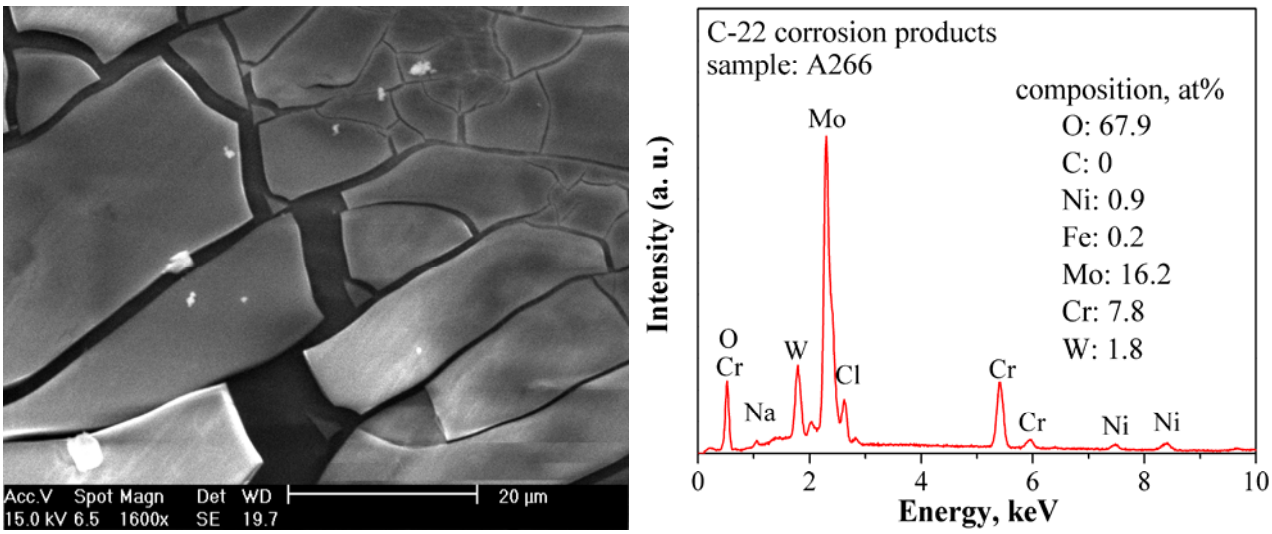

Fig. 10 SEM and EDS analysis of C-22 corrosion products under crevice former

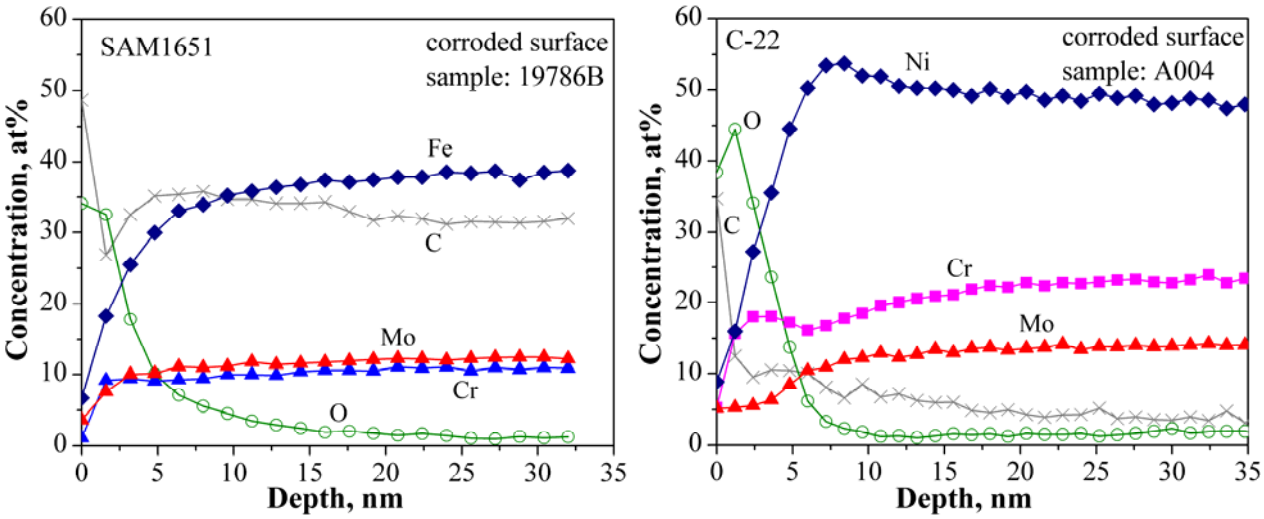

(a) (b)

Fig. 11. AES composition depth profile of (a) corroded SAM1651 and (b) C-22 surfaces